Geomagnetically Induced Currents at Middle Latitudes: 1. Quiet-time Variability

A. C. Kellerman[1], Ryan Mcgranaghan[2], Jacob Bortnik[3], Brett A. Carter[4], Joseph Hughes[2], Robert F. Arritt[5], Karthik Venkataramani[2], Charles H. Perry[5], Jackson McCormick[6], Chigomezyo M. Ngwira [2], Morris Cohen [6], Jia Yue [7 8]

[1]Department of Earth, Planetary, and Space Sciences, University of California, Los Angeles, USA
[2]ASTRA, LLC, 282 Century Place Suite 1000, Louisville, Colorado, USA.
[3]Department of Atmospheric and Oceanic Sciences, University of California, Los Angeles
[4]School of Science, RMIT University, Melbourne, Victoria Australia
[5]Technical Executive, Electric Power Research Institute
[6]School of Electrical Engineering, Georgia Institute of Technology. Atlanta, Georgia, USA
[7]NASA Goddard Space Flight Center, Greenbelt, MD USA
[8]Catholic University of America, DC USA

Key Points:

- Quiet-time GIC at middle latitudes follows a diurnal and annual cycle with quantifiable variability.
- Middle-latitude GIC observations are sensitive to quiet-time magnetic perturbations associated with the Sq current.
- GIC QDCs provide a robust baseline for significance analysis of GICs during geomagnetically disturbed times.

Corresponding author: Adam C. Kellerman, akellerman@epss.ucla.edu

Abstract

Geomagnetically induced current (GIC)s at middle latitudes have received increased attention after reported power-grid disruptions due to geomagnetic disturbances. However, quantifying the risk to the electric power grid at middle latitudes is difficult without understanding how the GIC sensors respond to geomagnetic activity on a daily basis. Therefore, in this study the question "Do measured GICs have distinguishable and quantifiable long- and short-period characteristics?" is addressed. The study focuses on the long-term variability of measured GIC, and establishes the extent to which the variability relates to quiet-time geomagnetic activity. GIC quiet-day curves (QDC)s are computed from measured data for each GIC node, covering all four seasons, and then compared with the seasonal variability of Thermosphere-Ionosphere- Electrodynamics General Circulation Model (TIE-GCM)-simulated neutral wind and height-integrated current density. The results show strong evidence that the middle-latitude nodes routinely respond to the tidal-driven Sq variation, with a node-specific dependence upon the direction of the ionospheric currents. The strong dependence of the GIC on the Sq currents demonstrates that the GIC QDCs may be employed as a robust baseline from which to quantify the significance of GICs during geomagnetically active times and to isolate those variations to study independently. The QDC-based significance score computed in this study provides power utilities with a node-specific measure of the geomagnetic significance of a given GIC observation. Finally, this study shows that the power grid acts a giant sensor which is sensitive to ionospheric current systems, even at middle latitudes.

1 Introduction

Solar storms result in an eruption of charged particles through flares and coronal mass ejections, which propagate through interplanetary space, and may eventually impact the Earth's magnetosphere. Energy transfer from the solar wind to the magnetosphere drives magnetospheric and ionospheric currents, and consequently, perturbations in the geomagnetic field. These geomagnetic field variations generate a surface geoelectric field via the electromagnetic induction process (Viljanen & Pirjola, 1994; Pirjola, 2000). The generation of these geoelectric fields occurs due to telluric currents flowing through the sub-surface structure of the Earth. When the impedance of naturally occurring subsurface material (e.g., rock) is high, geomagnetically induced currents (GIC)s will preferentially flow through human-made conductors, such as power systems and pipelines, leading to disruption of the power systems. It is therefore necessary to understand how GICs respond to geomagnetic activity in order to mitigate risk due to GIC (Pulkkinen et al., 2005; Guillon et al., 2016).

Water vapor and ozone absorption of solar radiation in the troposphere and stratosphere results in upward propagating atmospheric tidal waves, leading to global-scale oscillations with harmonic periods of a solar day (Chapman & Lindzen, 1970). These waves drive significant short-term variability in the neutral wind fields within the ionospheric dynamo region from 90 to 150 km (Miyahara & Ooishi, 1997). During quiet times, this variability is manifested in geomagnetic observations and is known as the solar quiet (Sq) variation (Graham, 1724b, 1724a; Stewart, 1882; van Sabben, 1964; Campbell & Matsushita, 1982; Campbell et al., 1993). The neutral wind field responds to the atmospheric tides, dragging the electrically conducting fluid through the Earth's magnetic field in the dynamo region to generate electromotive forces via wind-dynamo theory (Richmond, 1979). The dynamo generates electric currents that manifest as two large-scale vortices centered at middle to low latitudes (below $\sim$ 60°) - a counter-clockwise rotation in the northern hemisphere, and a clockwise rotation in the southern hemisphere - and are known as the Sq current.

During strong storms, there have been reports of power-grid disturbance at middle latitudes (Koen & Gaunt, 2002; Ngwira et al., 2008; Zois, 2013). Indeed, areas at mid-

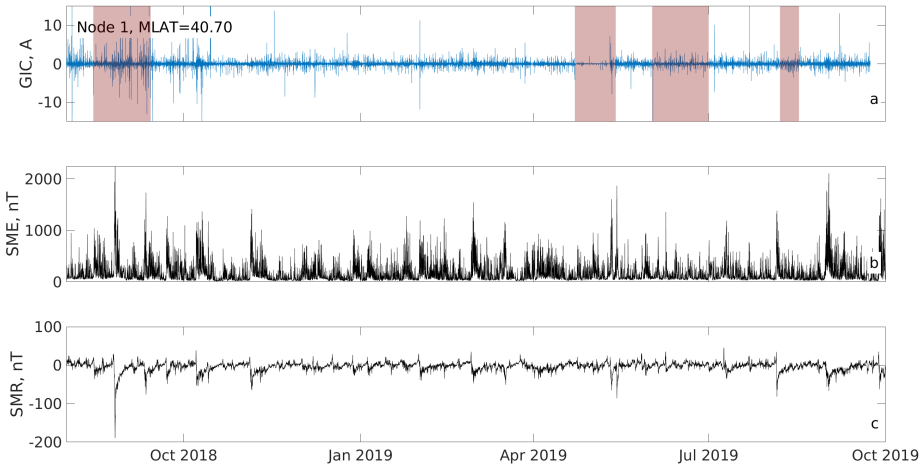

Figure 1. Line plot of measured current flowing into a transformer on the U.S. west coast, (b) SME, and (c) SMR vs time of year. The red shaded region indicates down time (see text for details). The geomagnetic latitude of the station is given

dle and low latitudes previously considered to be low risk to GIC, have experienced disruptions (Gaunt & Coetzee, 2007), and hence are an important factor when considering the general hazard to the electric power grid (Pulkkinen et al., 2017). Understanding the risk leading to GIC at middle latitudes depends on the nature of the response to geomagnetic activity measured by GIC sensors, including the day-to-day variability which is important for establishing the baseline response.

The question addressed in this study is whether the GIC nodes respond to the long-term, quiet-day oscillations, and to what extent the observed GIC response can be quantified. Quantifying the quiet-day component is important to distinguish the long-term variability from any short-term response, the latter of which may be due to elevated geomagnetic activity. By establishing the long-term baseline response, one can also quantify the significance of any short-term response and establish the relationship to geomagnetic activity.

The structure of the paper is as follows: Section 2 introduces the datasets and quiet-day curve classification criteria; Section 3 investigates the diurnal and annual variability of the GIC data and presents a comparison with Thermosphere-Ionosphere-Electrodynamics General Circulation Model (TIE-GCM) simulations of the neutral wind and height-integrated ionospheric current densities; Sections 5 and 6 discuss and conclude the paper.

2 Data Preparation and Quiet-day Classification

In this study, geomagnetic activity is specified by the SuperMAG auroral- electrojet (SME) (Newell & Gjerloev, 2011) and ring-current (SMR) (Newell & Gjerloev, 2012) indices. SuperMAG is a worldwide collaboration of organizations and national agencies that operate hundreds of magnetometers, and provide access to a unified dataset and indices (Gjerloev, 2012). Quiet geomagnetic periods are classified as times where SME $<$ 100 nT and $|\mathrm{SMR}| < 15$ nT. The GIC data provided for this study are transformer-level observations and part of the Sunburst network. The Electric Power Research Institute's (EPRI's) SUNBURST network program has proven to be an effective, organized approach for measuring, consolidating, and sharing data related to GIC (EPRI, 2018).

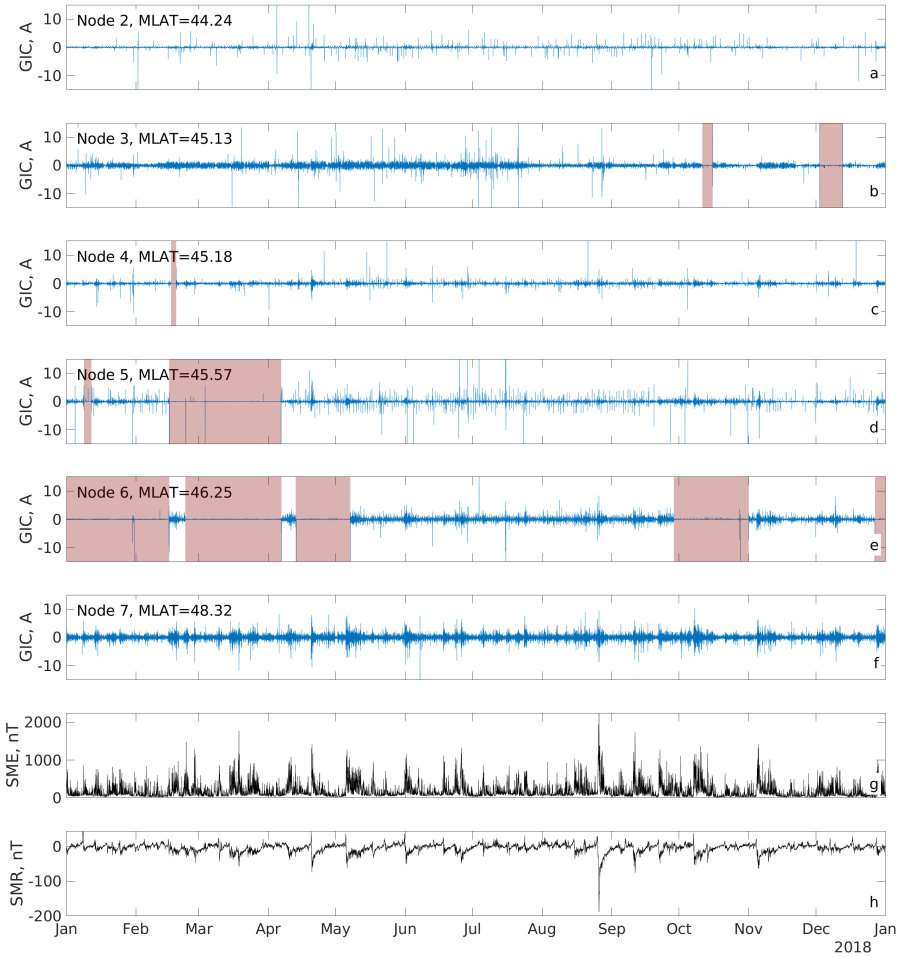

Figure 2. Similar to Figure 1 except for several nodes on the U.S. east coast.

A positive sign on the GIC current represents current flowing into transformers, and is measured at a cadence of 1 second. The names of individual nodes are excluded from this study for proprietary reasons, and instead, nodes are numbered in order of increasing magnetic latitude. The GIC nodes included in this study are located at magnetic latitudes between 40° and 50°.

Analysis of the GIC data revealed several periods in which the amplitude of current across multiple frequencies in the 1-50 mHz range were lower than other periods. In addition, sudden offsets with associated spikes in the data indicated non-geomagnetic-driven changes in the transformer operation. These periods were flagged as "downtime" and removed from the analysis. Figure 1 presents the GIC dataset from one US west-coast node, and illustrates a period of downtime by the shaded red region. Figure 2 illustrates the same data processing for several east-coast nodes. The difference in the time period in these two figures is a result of GIC data availability. For this study, data from Node 1 were available from August 2018 through October 2019, while data from Nodes 2 to 7 were available from January 2018 through December 2018.

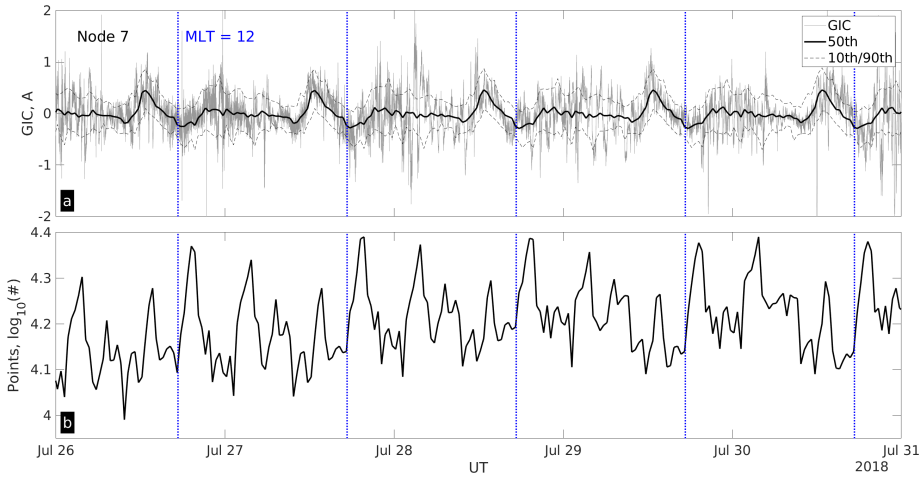

Figure 3. Example of the GIC QDC for Node 7 in July, 2018. The measured GIC is shown by the grey trace. The median, 10th and 90th percentiles are shown in the first panel. The second panel shows the log of the number of points included within each time interval.

The cleaned GIC data were averaged over 30-minute intervals for each day, and the same 30-minute interval from the preceding and superseding 10 days (i.e. 21-days of information) were used to compute the percentiles. Several other time intervals and steps were considered, including shorter averaging intervals. The shorter periods resulted in more structure in time, but the variability observed was largely within error (not shown here). The 30-minute interval results in a smooth estimation over the course of a day, while the 10-day period provides sufficient points from which to make the estimate. Little improvement is gained by incorporating more days, while statistical significance is reduced by reducing the number of days. The same technique was used for each available GIC node to produce a quiet-time curve (QDC) of measured current as a function of magnetic local time, and time of year. An example of the QDC technique applied to Node 7 for a period in July, 2018, is shown in Figure 3. The top panel shows the time of magnetic local time noon by the vertical dotted lines, the measured GIC in gray, and the 10th, 50th, and 90th percentiles by dashed, solid, and dashed lines, respectively. The bottom panel shows the logarithm of the number of valid points (matching the selection criteria). The high number of points confirms that the derived QDCs are statistically meaningful; the p-values were also found to be near zero, not shown here. A clear diurnal variation is evident in Figure 3a, with a significant pre-noon MLT GIC peak, and much of the finer-scale variability bounded by the 10th/90th percentiles. An example of a period of heightened GIC variability is shown on July 28, just after 0 UT, as defined by the GIC exceeding the QDC threshold.

3 Observations and Modeling

Two quiet-day curve computations, utilizing the median-based QDC approach, are illustrated in Figures 4 and 5, for the nodes at magnetic latitudes 40.7 and 48.32, respectively. Each figure shows the binned value of (a) solar-zenith angle at the node location, and (b) the GIC QDC, with the binning conducted over the time of year and magnetic local time. The solar zenith angle (SZA) is representative of the source of energy, the solar heating of the thermosphere, which drives quiet-time variability at middle and low latitudes. The solar heating drives both the diurnal and semi-diurnal tides, with the to-

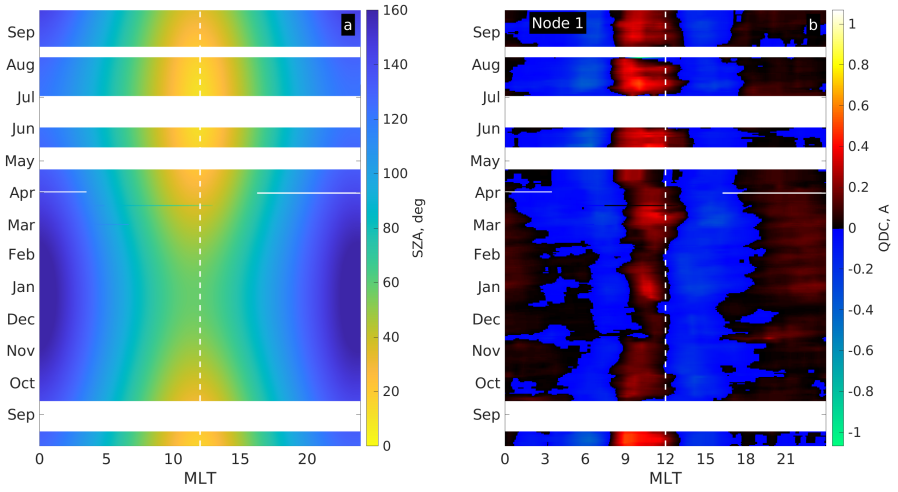

Figure 4. Node 1 (a) SZA vs time vs MLT and (b) GIC QDC

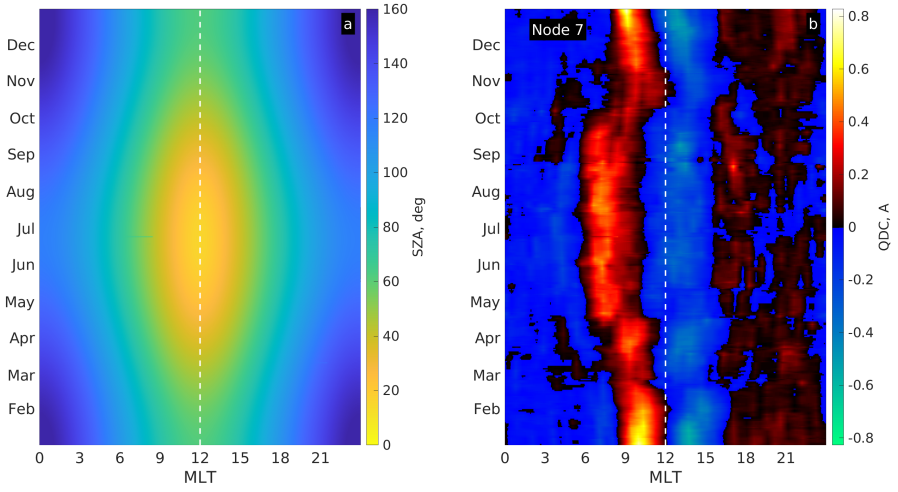

Figure 5. Node 7 (a) SZA vs time vs MLT and (b) GIC QDC

tal contribution from semi-diurnal tides dominating the heating in the lower ionosphere (Hagan et al., 2001). However, the phase of the semi-diurnal tides depends upon altitude, as the waves propagate away from the location of absorption. Hence, we do not look for a one-to-one agreement with SZA and GIC, but rather an observed change with season that implies the solar heating is the primary source of the observed variation.

Figures 4 and 5 exhibit similar QDC distributions, with clear seasonal variability in the the GIC magnitude and daily variability. Note that Figure 4 covers the period August 2018 through October 2019, while Figure 5 covers January 2018 through December 2018. In both figures, the peak-positive GIC occurs pre noon. Also evident in both figures is (a) a transition to negative GIC near 12 MLT, and (b) a negative to positive reversal at around 18 MLT. The differences in the time and structure of the GIC QDCs are addressed below. The observed variability in the GIC QDC appears to be semi-diurnal, though the peak amplitude appears to be diurnal in nature.

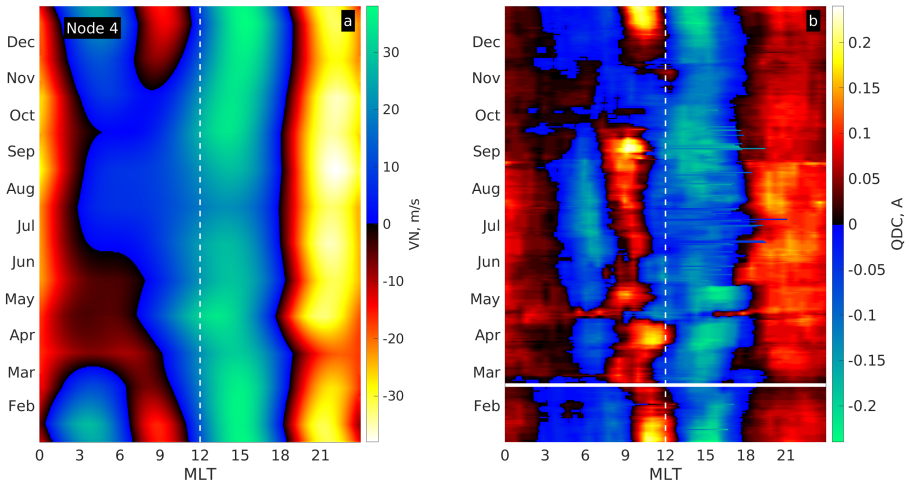

Figure 6. Binned value plot of (a) TIE-GCM-modeled meridonal neutral wind velocity (VN) and (b) GIC QDC at Node 4. Each quantity is plotted versus time of year and magnetic local time. Neutral winds from 100-120 km geometric height at model midpoints are considered.

The observed seasonal dependence of the GIC QDCs may match the Sq variability. In order to investigate this in detail, two year-long simulations using the TIE-GCM v2.0 model (Qian et al., 2014) were conducted for 2018 and 2019. The TIE-GCM is a self consistent numerical model of the thermosphere which includes the dynamics, energetics and chemistry with a steady-state ionospheric electrodynamo in a realistic geomagnetic main field (Richmond et al., 1992; Qian et al., 2014). The model spans from approximately 97 km to 450 to 600 km, though the model uses log pressure $Z = ln(p_0/p)$ as the vertical coordinate with the reference pressure p_0 set to $p_0 = 5{\times}10^{-7}$ hPa, and hence varies with solar activity. The ionospheric electrodynamics are calculated in a modified magnetic Apex coordinate system (Richmond, 1995). In this study, the model runs were conducted at 5-degree resolution, using a 60-second time step, constant F10.7 = 71, Kp = 2.0, climatological GSWM diurnal and semi-diurnal migrating tides (Hagan et al., 2001), Heelis et al. (1982) high-latitude potential model, aurora parameterization enabled, an O-O+ collision factor of 1.5, electro-dynamo enabled, height-integrated and plasma pressure gradient currents enabled, and calculation of helium enabled. The model outputs were linearly interpolated to the location of each node for the analysis that follows.

Figure 6 displays the height-averaged (100-120 km geometric height at model midpoints) TIE-GCM-modeled meridional neutral wind and measured GIC QDC at Node 4. In the NH winter months, the MLT-dependent transitions in the meridional wind correspond well with transitions in the GIC, albeit with some small differences. In the NH summer months, however, the early afternoon and dusk transitions occur at similar MLT (the 12-24 MLT sector), however the morning transitions in GIC exhibit more structure, including a peak in GIC, that is not associated with a negative meridional wind in the lower ionosphere.

The tidal-driven wind-dynamo drives currents in the ionosphere leading to perturbations at the Earth's surface (Richmond, 1979), which may drive the low amplitude GICs observed in Figure 6. The neutral winds vary in direction and magnitude as height increases into the dynamo region, and hence the average wind field may not capture combined effects leading to GIC in the power grid. Further, the differences in the observed

GIC at each location are likely a result of the complexity and orientation of the interconnected power grid, and subsurface conductivity structure. Therefore, the contribution to the GIC may be better analyzed by considering components of the height-integrated horizontal currents. The TIE-GCM model allows to compute height-integrated current densities $K_{q\phi}$ and $K_{q\lambda}$ (Richmond, 1995), representing the east and north directions, respectively.

A comparison between the TIE-GCM-modeled height-integrated horizontal current density and the measured GIC is presented in Figure 7 for five nodes. In order to account for potential differences in the aforementioned grid configuration and sub-surface conductivity structure, influence and orientation factors are introduced here. The height-integrated horizontal current K_q is computed from the following equation $K_q = a(K_{q\phi}) + b(K_{q\lambda})$, with $|a| + |b| = 1$, and where a and b control the relative importance of the east-west and north-south components, respectively, as well as the direction (positive east and north). The introduction of these factors allows one to find a height-integrated ionospheric current configuration which most closely matches the observed GIC, and hence determine the direction most likely to drive positive GICs at each node. The a and b are indicated for each node in Figure 7, and found numerically. The numerical solution minimizes the mean-absolute error between the normalized GIC and K_q.

Figure 7a presents K_q at Node 1, resolved to be positive in the south-west direction ($a = -0.13, b = -0.87$), with 13 % contribution from the west current and 87 % from the south current; the corresponding GIC is shown in Figure 7b, and the absolute error of the normalized GIC and K_q is shown in Figure 7c. The general shape of the positive K_q resembles the GIC from 9-24 MLT, with a narrow region of enhanced K_q in winter, and a wider region in the NH summer. In the summer-morning sector (0 –9 MLT), the agreement is not well aligned in MLT, with a noticeably wider region of positive K_q. The mean absolute error is 0.17.

Figure 7d displays K_q at Node 2, resolved to be positive in the south-west direction. In this case, the region of positive K_q generally matches that of the GIC in Figure 7e, though there are some discrepancies between the extent in MLT of the K_q post dawn and in the early afternoon, with K_q again showing an earlier transitions in NH summer.

Figure 7g displays K_q at Node 4, resolved to be positive in the south-east direction. Here, a near-equal ($a = 0.52$) east and ($b = -0.48$) south current contribution is used. The K_q transitions match those from the GIC in Figure 7h during the NH winter months, however in the summer months, the GIC exhibits more structure post dawn as seen by the strong positive absolute error in Figure 7i near 6 MLT. The discrepancy is similar to what was seen in Figure 6, and Figure 7c. The agreement between the K_q and GIC transitions is good from the pre-noon to dusk sector, with absolute error values less than 1.

Figure 7j displays K_q at Node 5, resolved to be positive in the south-west direction. A 6% east current contribution is resolved (mostly meridional and similar to Node 1). Similar to Figure 7a, the K_q transitions match those from the GIC in Figure 7k during the NH winter months, however in the summer months the MLT extent of K_q is larger and, in Figure 7l, a clear positive error near 6 MLT is observed.

Finally, Figure 7m displays K_q at Node 7, resolved to be positive in the south-east direction. Similar to Figure 7g, nearly equal ($a = 0.51$) east and ($b = -0.49$) south current contributions are found to best align K_q and GIC. The agreement between K_q and GIC in Figure 7n is very good across all months, as borne out by the low absolute error values in Figure 7o, although the K_q does turn positive at a slightly earlier MLT than GIC in NH summer, and the negative K_q appears to be too strong for the observed GIC response.

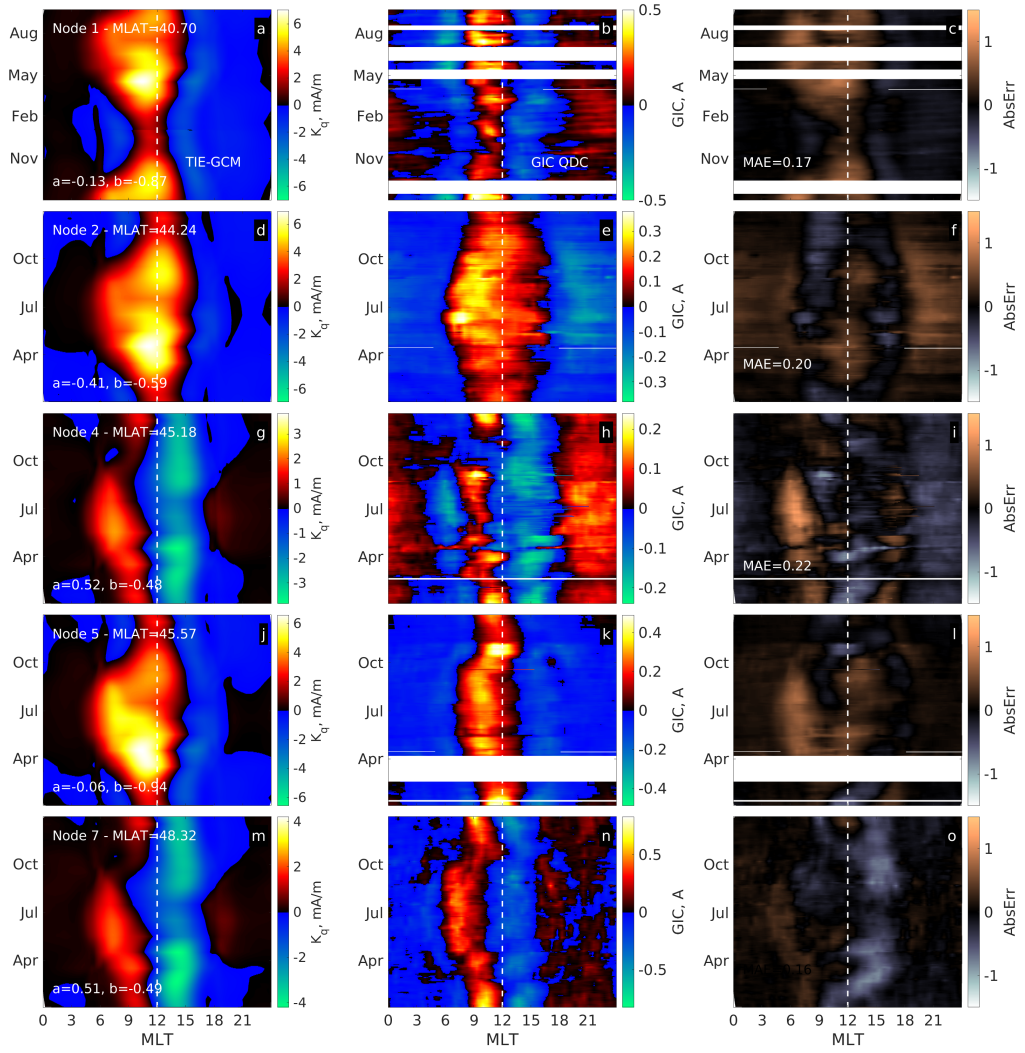

Figure 7. Binned value plot of the height-integrated 1-D current density, GIC QDC, and the absolute error between the normalized values of GIC and current density. The mean absolute error is shown for each node. See text for details.

In summary, Figure 7 illustrates a striking similarity between the height integrated currents and the GIC. A clear relationship is evident between the daily variability of the ionospheric currents and the GIC, and the variability in both throughout the year. The direction and magnitude of the zonal (east) and meridional (north) components are shown to be a critical factor determining the quiet-day response of these nodes. This directional dependence may also provide insight into how each GIC node may respond during active times. At nodes where meridional winds dominate the GIC ($|a| << |b|$), the MAE indicated that a northward directed wind may be not fully captured by the TIE-GCM model near 6 MLT and near summer; a region of negative GIC was routinely observed for each of these nodes in Figure 7. In the next section, the QDC-GIC values are employed in an example event to demonstrate their value during geomagnetically active times.

4 GIC During a Geomagnetically Active Period

In this section, the quiet-time component of the GIC response is used to compute a baselined GIC response, which contains only the active-time component. The baselined GIC data are then used to infer the true impact of geomagnetic activity on the GIC response for a specific period of time. The baselined GIC value is thus $\mathrm{GIC_{BL}} = \mathrm{GIC_{obs}} - \mathrm{QDC_{50}}$, where $\mathrm{GIC_{obs}}$ are the observed GIC values, and $\mathrm{QDC_{50}}$ is the 50th percentile of the QDC distribution. The significance is computed by way of a percentile-based inter-percentile range (IPR) z score, defined in terms of the 10th or 90th percentile as follows

$$\mathrm{z_{IPR}} = \begin{cases} \mathrm{GIC_{BL}}/\delta_{90}, & \text{if } \mathrm{GIC}_{obs} \geq 0 \\ \mathrm{GIC_{BL}}/\delta_{10}, & \text{otherwise} \end{cases}$$

where $\delta_{90} = \mathrm{QDC_{90}} - \mathrm{QDC_{50}}$ and $\delta_{10} = \mathrm{QDC_{50}} - \mathrm{QDC_{10}}$. The subscripts 10 and 90 refer to the time-dependent 10th and 90th percentiles of the QDC distribution. The $\mathrm{z_{IPR}}$ hence provides a robust measure of significance for either negative or positive GIC observations, which reliably and repeatably isolates the GMD-related GIC.

Figure 8 presents a moderate storm period in August 2018. Three events are highlighted in Figure 8, in green, blue and red. The first event in green identifies a period of calm prior to the storm. The second event in blue highlights a sharp increase in dynamic pressure, which is shown in Figure 8b. The third event in red highlights the sharp increase in SME, which is shown in Figure 8a, and an a period of high solar wind velocity, as shown in Figure 8c. Figure 8d presents the observed GIC from Node 6 for this period, with the QDC 10, 50, and 90 percentiles over plotted. The baselined GIC values are shown in Figure 8e, and the significance score is shown in Figure 8f.

In Figure 8d the observed GIC exhibits peaks of $\sim$ 2A in events 1 and 3, and a negligible response to event 2. Figure 8d illustrates that the quiet-time component contributes $\sim$ 1A to GIC in event 1, and $\sim$ 0A in events 2 and 3. The baselined GIC $\mathrm{GIC_{BL}}$ in Figure 8e represents the active component of the GIC response, and illustrates that the active component contributes $\sim$ 1A to event 1, approximately 0.5A to event 2, and nearly the entire 2A to event 3. One can conclude that the GIC response observed in event 3 was due to enhanced geomagnetic activity. The significance of the GIC response, as it pertains to geomagnetic active time, is illustrated in Figure 8f. The z-score confirms that the variability in event 1 is much less significant ($\sim$ 5) than event 2 ($\sim$ 10), with regards to elevated geomagnetic activity.

The significance scores for nodes 2 to 7 are presented together in Figure 9 for the same period of time. For each node, the significance is higher during event 3 than event 1, revealing that enhanced geomagnetic activity is responsible for a significant response across all nodes. Interestingly, several nodes also show a significant response during event 2, simultaneous with the increase in dynamic pressure. Although only a single period has been shown here, these results demonstrate that the QDCs are a powerful dataset from which quantify the impact of geomagnetic activity on the electric power grid.

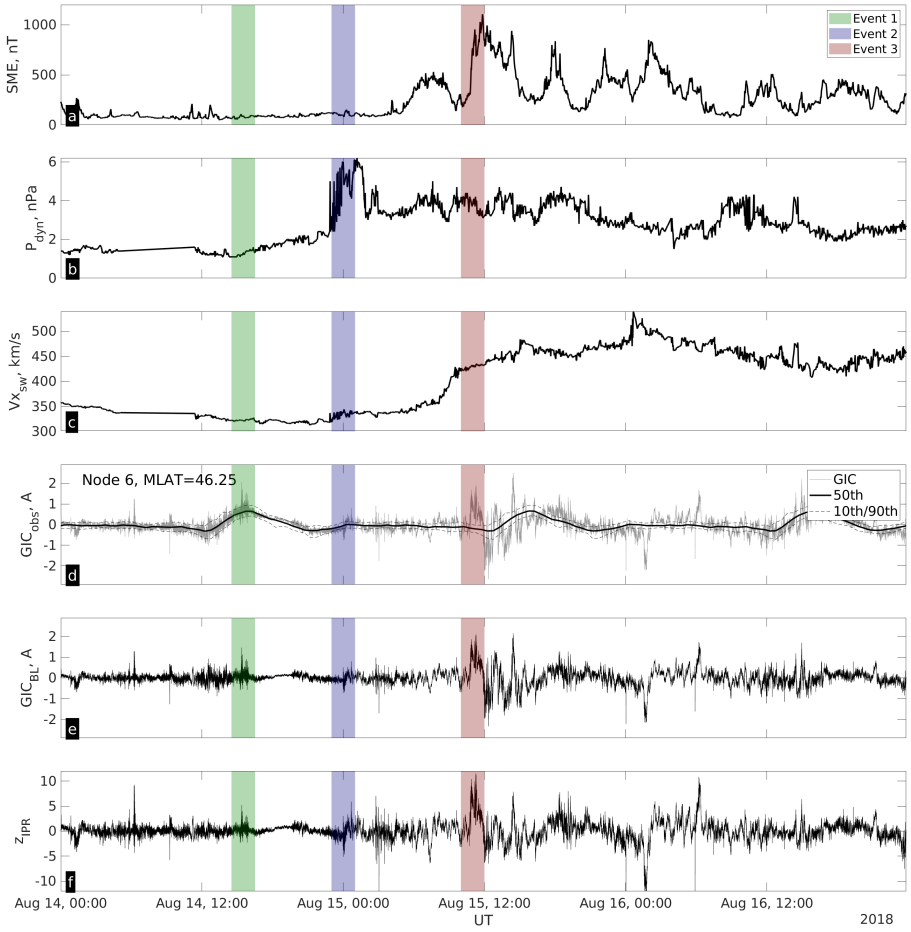

Figure 8. Line plots of a moderate storm period, focused on Node 6, displaying (a) SME, (b) Observed GIC, (c) QDC-baselined GIC, and (d) inter-percentile range z-score, versus UT. Two events of interest are highlighted in green and blue.

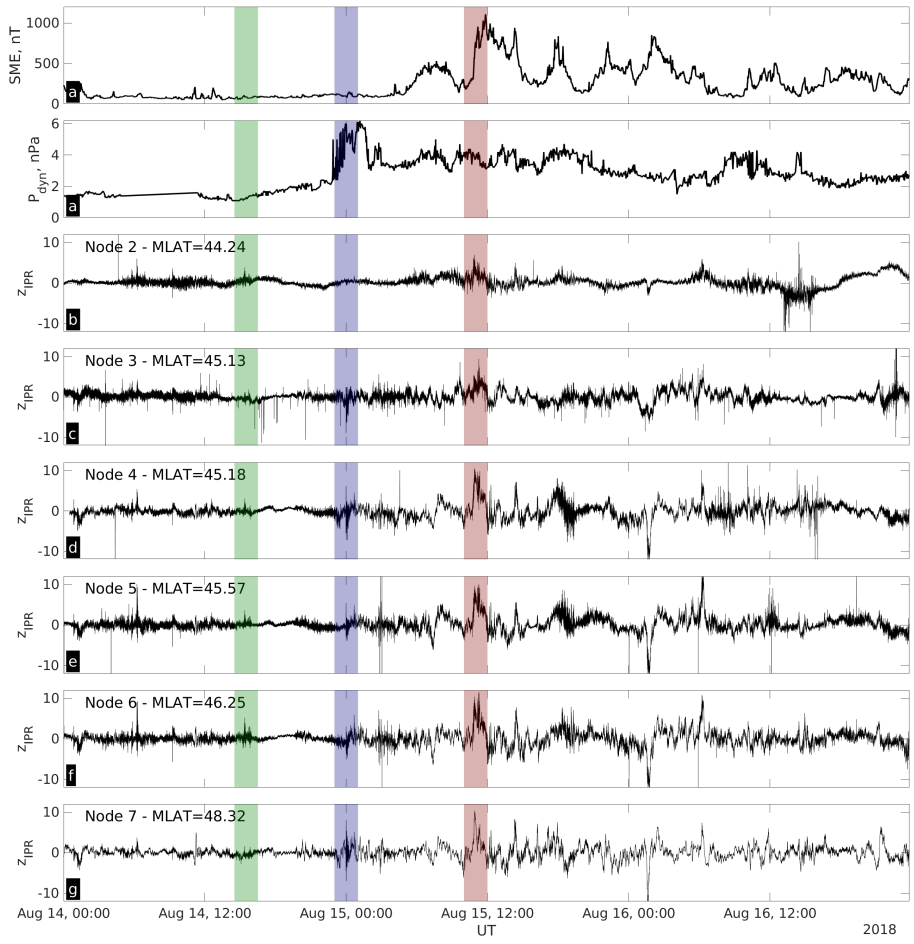

Figure 9. Line plots of SME and significance for Nodes 2 through 7. See text for details.

5 Discussion

The TIE-GCM simulations in Figures 6 and 7 illustrate the good agreement between the tidal-driven Sq current and the observed quiet-day perturbations in the GIC detected at several transformer locations at middle latitudes. The identified dependence on the direction of the height-integrated horizontal currents provide a node-specific estimate of the direction leading to positive GIC at each node location. The magnitude of the response exhibits a clear MLT dependence, which is important for accurately specifying the effect of geomagnetic storms on GIC currents, as shown in Figures 8 and 9.

A discrepancy between K_q and the quiet-day component of the GIC is identified in NH summer, near dawn for several nodes, where a positive K_q corresponds to a negative quiet-day GIC; a transition to positive quiet-day GIC occurs later each morning. Given the orientation flags used ($b < 0$), this suggest that a period of stronger northward meridional winds may not be fully represented in the TIE-GCM model during NH summer, and in the post-dawn sector However, the overall good agreement between the Sq variation and the GICs supports the idea that the migrating tidal-driven perturbations in ionospheric currents are responsible for the quiet-time variability in the GICs.

The dependence of each node on a particular orientation of the height integrated current density K_q, is consistent with the notion that information on the grid configuration is potentially as important as the GIC observations themselves. For instance, Nodes 1 and 5 show similar seasonal variability and orientation flags, though Node 1 is located on the U.S. west coast at 40.7 deg MLAT, while Node 5 is located on the east coast at 45.57 deg MLAT. Whereas Nodes 4 and 5 show very different seasonal variability, though both nodes are located on the east coast within 1 deg MLAT of each other. Indeed, past analysis of the GIC response at middle-latitude in New Zealand revealed different transformer-level GIC responses within the same substation (Mac Manus et al., 2017). The strong dependence on the orientation of the height-integrated currents presented here confirms the importance of the grid configuration in the GIC response.

Since global geomagnetic disturbances comprise the quiet (Sq) and disturbance (Dst) components of the geomagnetic field, the good agreement between GICs and the Sq variation suggests that the QDCs provide a suitable (Sq) baseline from which to define the significance of the observed GIC during active times, and hence a robust method to quantify the effects of geomagnetic disturbance (GMD) on the electric power grid. This methodology was applied to investigate the GIC response during one time period, as shown in Figures 8 and 9. The analysis demonstrated that the largest, active-component GIC measured during this period could be attributed to perturbations at 40 to 80 deg MLAT, demonstrating the capability to estimate the significance of geomagnetic activity on any observed GIC. The techniques applied to derive a QDC for the GIC may be applicable to any node, however, the specifics of the analysis with regards to Sq variation are most applicable to latitudes equatorward of the auroral region, and poleward of the equatorial fountain.

This section will conclude by noting several aspects of the current work which are useful for power utilities: (1) By defining the expected GIC behavior during quiet times, QDC's provide a robust baseline which operators may use to ensure their GIC monitors are operating nominally, (2) Identification of the dominant ionospheric current direction leading to positive GIC at each node can help understand the risk to that node during an active event (theoretical or real, and provided the grid configuration is the same), (3) GIC modeling may be tested during quiet times, as we have a very good understanding of the geomagnetic drivers and the expected GIC response - this may help to improve GIC modeling during active times. (4) The significance score computed in this study provides power utilities with a measure of the geomagnetic significance of a given GIC perturbation, which could be applied in real time.

6 Conclusions

In this study, GIC measurements from several middle-latitude nodes and SuperMAG geomagnetic indices were used to develop quiet-day curves for geomagnetically induced currents. The potential driver of the observed variability in each QDC was investigated by employing the TIE-GCM model, leading to the following conclusions:

1. Quiet-time GIC observations exhibit quantifiable variability that depends on magnetic local time and season.

2. The quiet-time GIC matches well with daily and seasonal changes in height-integrated horizontal currents above each node location, and hence are attributed to the Sq current system. The direction of the currents is an important factor in determining the impact of the ionospheric currents on any given GIC node. These results show that the power grid may be used as a giant sensor for ionospheric currents at middle latitudes.

3. Given that GIC nodes respond to the quiet-time Sq variation, the GIC QDCs may be used as a robust baseline to define the significance of GIC measurements during geomagnetically disturbed times.

Acknowledgments

The data provided for this study are part of the Sunburst network. We are currently not able to release the GIC data directly, due to agreements with EPRI and the power utilities who provided data for this analysis, however, by acceptance, we will post the simulation results and GIC-QDC data on `https://zenodo.org`. We gratefully acknowledge the SuperMAG collaborators (`https://supermag.jhuapl.edu/info/?page=acknowledgement`) for the indices employed in this study available at `https://supermag.jhuapl.edu/indices`. We acknowledge use of NASA/GSFC's Space Physics Data Facility's OMNIWeb service, and OMNI data available at `https://omniweb.gsfc.nasa.gov`. We acknowledge the developers of the TIE-GCM model, available at `https://www.hao.ucar.edu/modeling/tgcm/tie.php`. Simulation analysis was assisted by the Community Coordinated Modeling Center at Goddard Space Flight Center (http://ccmc.gsfc.nasa.gov). We acknowledge the developers of the IRBEM library, which was utilized to obtain magnetic coordinates in the study. ACK and JB were supported by NSF grant 1937152. RMM was supported by NSF grants 1937152 and 1940208. BAC was supported by the Australian Research Council's Linkage Project scheme (LP160100561).

References

Campbell, W. H., Arora, B. R., & Schiffmacher, E. R. (1993). External sq currents in the india-siberia region. *Journal of Geophysical Research: Space Physics*, *98*(A3), 3741-3752. Retrieved from `https://agupubs.onlinelibrary.wiley.com/doi/abs/10.1029/92JA02552` doi: https://doi.org/10.1029/92JA02552

Campbell, W. H., & Matsushita, S. (1982). Sq currents: A comparison of quiet and active year behavior. *Journal of Geophysical Research: Space Physics*, *87*(A7), 5305-5308. Retrieved from `https://agupubs.onlinelibrary.wiley.com/doi/abs/10.1029/JA087iA07p05305` doi: https://doi.org/10.1029/JA087iA07p05305

Chapman, S., & Lindzen, R. S. (1970). *Atmospheric tides.* Springer Netherlands. (An optional note)

EPRI. (2018). *SUNBURST Network Membership.*

Gaunt, C. T., & Coetzee, G. (2007). Transformer failures in regions incorrectly considered to have low gic-risk. In *2007 ieee lausanne power tech* (p. 807-812).

Gjerloev, J. W. (2012, September). The SuperMAG data processing technique. *Journal of Geophysical Research (Space Physics)*, *117*(A9), A09213. doi: 10.1029/2012JA017683

Graham, G. (1724a). Iii. observation of the dipping needle. made at london, in the beginning of the year 1723. *Philosophical Transactions of the Royal Society of London*, *33*(389), 332-339. Retrieved from https://royalsocietypublishing.org/doi/abs/10.1098/rstl.1724.0062 doi: 10.1098/rstl.1724.0062

Graham, G. (1724b). Iv. an account of observations made of the variation of the horizontal needle at london, in the latter part of the year 1772, and beginning of 1723. *Philosophical Transactions of the Royal Society of London*, *33*(383), 96-107. Retrieved from https://royalsocietypublishing.org/doi/abs/10.1098/rstl.1724.0020 doi: 10.1098/rstl.1724.0020

Guillon, S., Toner, P., Gibson, L., & Boteler, D. (2016, Nov). A colorful blackout: The havoc caused by auroral electrojet generated magnetic field variations in 1989. *IEEE Power and Energy Magazine*, *14*(6), 59-71. doi: 10.1109/MPE.2016.2591760

Hagan, M. E., Roble, R. G., & Hackney, J. (2001). Migrating thermospheric tides. *Journal of Geophysical Research: Space Physics*, *106*(A7), 12739-12752. Retrieved from https://agupubs.onlinelibrary.wiley.com/doi/abs/10.1029/2000JA000344 doi: https://doi.org/10.1029/2000JA000344

Heelis, R. A., Lowell, J. K., & Spiro, R. W. (1982). A model of the high-latitude ionospheric convection pattern. *Journal of Geophysical Research: Space Physics*, *87*(A8), 6339-6345. Retrieved from https://agupubs.onlinelibrary.wiley.com/doi/abs/10.1029/JA087iA08p06339 doi: https://doi.org/10.1029/JA087iA08p06339

Koen, J., & Gaunt, C. T. (2002). Geomagnetically induced currents at mid-latitudes. In *International union radio science (ursi) general assembly, maastrich.*

Mac Manus, D. H., Rodger, C. J., Dalzell, M., Thomson, A. W. P., Clilverd, M. A., Petersen, T., ... Divett, T. (2017). Long-term geomagnetically induced current observations in new zealand: Earth return corrections and geomagnetic field driver. *Space Weather*, *15*(8), 1020-1038. doi: https://doi.org/10.1002/2017SW001635

Miyahara, S., & Ooishi, M. (1997, January). Variation of Sq Induced by Atmospheric Tides Simulated by a Middle Atmosphere General Circulation Model. *Journal of Geomagnetism and Geoelectricity*, *49*(1), 77-87. doi: 10.5636/jgg.49.77

Newell, P. T., & Gjerloev, J. W. (2011, December). Evaluation of SuperMAG auroral electrojet indices as indicators of substorms and auroral power. *Journal of Geophysical Research (Space Physics)*, *116*(A12), A12211. doi: 10.1029/2011JA016779

Newell, P. T., & Gjerloev, J. W. (2012). Supermag-based partial ring current indices. *Journal of Geophysical Research: Space Physics*, *117*(A5). Retrieved from https://agupubs.onlinelibrary.wiley.com/doi/abs/10.1029/2012JA017586 doi: 10.1029/2012JA017586

Ngwira, C. M., Pulkkinen, A., McKinnell, L.-A., & Cilliers, P. J. (2008). Improved modeling of geomagnetically induced currents in the south african power network. *Space Weather*, *6*(11). doi: 10.1029/2008SW000408

Pirjola, R. (2000, December). Geomagnetically induced currents during magnetic storms. *IEEE Transactions on Plasma Science*, *28*(6), 1867-1873. doi: 10.1109/27.902215

Pulkkinen, A., Bernabeu, E., Thomson, A., Viljanen, A., Pirjola, R., Boteler, D., ... MacAlester, M. (2017). Geomagnetically induced currents: Science, engineering, and applications readiness. *Space Weather*, *15*(7), 828-856. Retrieved from https://agupubs.onlinelibrary.wiley.com/doi/abs/10.1002/2016SW001501 doi: 10.1002/2016SW001501

Pulkkinen, A., Lindahl, S., Viljanen, A., & Pirjola, R. (2005). Geomagnetic storm of 29–31 october 2003: Geomagnetically induced currents and their relation

to problems in the swedish high-voltage power transmission system. *Space Weather*, *3*(8). doi: 10.1029/2004SW000123

Qian, L., Burns, A. G., Emery, B. A., Foster, B., Lu, G., Maute, A., ... Wang, W. (2014). The NCAR TIE-GCM. In *Modeling the ionosphere–thermosphere system* (p. 73-83). American Geophysical Union (AGU). Retrieved from `https://agupubs.onlinelibrary.wiley.com/doi/abs/10.1002/9781118704417.ch7` doi: https://doi.org/10.1002/9781118704417.ch7

Richmond, A. D. (1979). Ionospheric wind dynamo theory: A review. *Journal of geomagnetism and geoelectricity*, *31*(3), 287-310. doi: 10.5636/jgg.31.287

Richmond, A. D. (1995). Ionospheric electrodynamics using magnetic apex coordinates. *Journal of geomagnetism and geoelectricity*, *47*(2), 191-212. doi: 10.5636/jgg.47.191

Richmond, A. D., Ridley, E. C., & Roble, R. G. (1992). A thermosphere/ionosphere general circulation model with coupled electrodynamics. *Geophysical Research Letters*, *19*(6), 601-604. Retrieved from `https://agupubs.onlinelibrary.wiley.com/doi/abs/10.1029/92GL00401` doi: 10.1029/92GL00401

Stewart, B. (1882). Hypothetical views regarding the connection between the state of the sun and terrestrial magnetism. In (9th ed., Vol. 16, p. 181-184). The address of the publisher.

van Sabben, D. (1964). North-south asymmetry of sq. *Journal of Atmospheric and Terrestrial Physics*, *26*(12), 1187 - 1195. Retrieved from `http://www.sciencedirect.com/science/article/pii/0021916964901278` doi: https://doi.org/10.1016/0021-9169(64)90127-8

Viljanen, A., & Pirjola, R. (1994, July). Geomagnetically induced currents in the Finnish high-voltage power system. *Surveys in Geophysics*, *15*(4), 383-408. doi: 10.1007/BF00665999

Zois, I. P. (2013). Solar activity and transformer failures in the greek national electric grid. *Space Weather Space Climate*, *3*(A32). doi: 10.1051/swsc/2013055